Journal of Science and Sustainable Development (JSSD), 2023, 11(2), 45-62

ISSN: 2304-2702 (print); 2414-4479 (online)
DOI: https://doi.org/10.20372/au.jssd.11.2.2023.0464 [45]

RESEARCH PAPER

Surface Kinetic and Thermodynamic Behaviors of Cu-NiO/PANI Assisted Photodegradation of Tris(4-(Dimethylamino) Phenyl) Methylium Chloride (TDPM)

Tibebu Alemu, Taye Bekele, Girmaye Asefa, Bulti Abdisa Kerayu

Department of Chemistry, College of Natural and Computational Sciences, Ambo University, Ambo, Ethiopia

***Corresponding Author** Email: tibebu.alemu@ambou.edu.et*

Abstract

Environmental pollution and the contamination of drinking water become serious environmental challenges that are getting worldwide attention. As a result, scholars are developing effective treatment strategies to transform toxic pollutants into environmentally friendly compounds and safe for human health. This study investigated the influence of thermodynamics and kinetics on the photocatalytic degradation of crystal violet using Cu-NiO/PANI nanocomposites. The synthesized nanomaterials were characterized by X-ray diffraction (XRD), Fourier-transform infrared spectroscopy (FTIR), and Ultraviolet-visible spectroscopy (UV-Vis) spectrometers. The XRD results showed that NiO and Cu-NiO nanoparticles (NPs) and Cu-NiO/PANI nanocomposites (NCs) possessed crystalline structures. FTIR has confirmed that NiO and Cu-NiO NPs and Cu-NiO/PANI NCs were successfully prepared while the UV-Vis result indicated that the energy band gaps were decreased from 3.1 eV for NiO to 1.63 and 1.60 eV for Cu-NiO and Cu-NiO/PANI, respectively. The degradation of crystal violet at NiO, Cu-NiO, and Cu-NiO/PANI surfaces under different pH, initial dye concentration, and doses of photocatalyst, was examined. Among the photocatalysts, Cu-NiO/PANI was found to be a very effective photodegradation catalyst for the organic dye. The maximum decolorization achieved was 96.5% using Cu-NiO/PANI at pH 3, and 10 ppm initial concentration of dye, 120 min light irradiation, 110 mg catalyst dose, and 25 ˚C. The results indicate that the photodegradation of crystal violet dye follows pseudo-second-order kinetics and interestingly, the degradation efficiency decreased as the reaction temperature increased. This suggests that the reaction is exothermic, meaning it releases heat.

Keywords: Photocatalytic degradation. TDPM model dye, Cu-NiO/PANI nanocomposite, pseudo-second-order kinetics, thermodynamic parameters

Introduction

Contamination of drinking water has become a serious environmental hazard, attracting worldwide attention. Common toxic pollutants include dyes, heavy metals, nitrates, non-biodegradable wastes, pharmaceutical products, and toxic chemicals. These pollutants are being discharged into natural water bodies without adequate pre-treatment (Bonetto et al., 2015). Due to rapid industrialization and urbanization, these pollutants are increasing dramatically. Among these contaminants, organic dyes are particularly problematic. Their stability makes them difficult to biodegrade, causing severe water pollution. Organic dyes are used in various industries, including textiles, paper, dyeing, rubber, plastics, cosmetics, and leather tanning. The previous report indicates that the majority of organic dyes are toxic and carcinogenic, and cause the formation of hazardous byproducts through chemical reactions in wastewater bodies (Shah et al., 2019). The discharging of colored effluent imposes negative impacts as a result of its toxicological and esthetical behavior. In

addition, dyes and their by-products are also carcinogenic toxins that act as sources of water pollution and are harmful to aquatic life in water systems (Gürses et al., 2006). In addition to the aforementioned effects, organic dyes can also cause severe damage to humans, including malfunctioning of the kidneys, reproductive system, liver, brain, and central nervous system (Cazetta et al., 2011).

Cationic dyes are a major type of pollutant found in wastewater discharged from various industries, including dye production, pulp and paper mills, paint manufacturing, polymer production, herbicide production, and wood preservation. These dyes, such as crystal violet and malachite green, are difficult to break down into non-toxic molecules because they are resistant to oxidizing agents, light, heat, aerobic digestion, and photochemical degradation (Katheresan, Kansedo, & Lau, 2018). Therefore, scientists are developing strategies to transform toxic organic dyes into environmentally friendly compounds and safe for human health (Hajati et al., 2015). For example, ion exchange, adsorption, coagulation, flocculation, reverse osmosis, ultra-filtration membrane, advanced oxidation, and photo-catalysis are among common treatment techniques (Shah et al., 2019). In recent years, Advanced Oxidation Processes (AOPs) have gained significant recognition for their effectiveness in removing organic pollutants and improving water quality. Compared to traditional treatment methods, AOPs offer several key benefits (Saleh and Djaja, 2014). Among AOPs, heterogeneous photocatalysis with metal oxide semiconductor particles stands out for its efficiency in removing organic pollutants from wastewater. This technique utilizes direct solar energy to degrade the pollutants, resulting in no secondary contamination (Konstantinou and Albanis, 2004). The photo-degradation process using semiconductors such as ZnO, TiO2, Fe2O3, CdS, ZnS, and NiO are the most suitable owing to their quick oxidation pollutants and lack of formation of polycyclic products.

NiO nanoparticle (NP) has received great attention for the reason of its excellent physical and optical properties. NiO NP is a p-type semiconductor with a wide energy band gap of 3.6 to 4.0 eV at room temperature (Morin, 1954). The uniqueness in photosensitivity and catalytic properties makes it an efficient catalyst for the degradation of pollutants in the presence of UV light. NiO NP has been deemed as a promising material for the remediation of hazardous wastewater, as a result of its high activity, powerful oxidation, non-toxicity, chemical stability (Bhat et al., 2020), low cost, and environmentally friendly features. Doping the photocatalyst with metals or a combination of metals (co-doping) significantly improves its ability to degrade dye molecules. This enhancement occurs because doping reduces the recombination of electron-hole pairs, which are crucial for the degradation process (Imran et al., 2021), and enhances the chemical reaction to take place for the disintegration of organic pollutants into CO2 and H2O. Doping selective metal ions such as copper (Cu) can increase the surface defects and shift the light absorption towards the visible region (Saleh and Djaja, 2014) and such metal ions may cause NiO to get smaller in particle size, allowing charge carriers to travel easily and minimize the recombination effect. Additionally, the incorporation of Cu metal can provide unique optical properties, such as plasmon resonance for NiO NP which can be beneficial for applications in sensors, imaging, optoelectronic devices, and photo-catalytic activity (Karthik et al., 2022). Even though, researchers are intensively working on the photocatalytic remediation of dye-polluted wastewater; the efficiency of the photodegradation process needs immense efforts to overcome the rapid electron-hole recombination rate and limited light absorbance spectrum.

To improve the photocatalytic efficiency of these semiconductors, researchers have incorporated a conductive polymer for instance polyaniline (PANI) which facilitates the narrowing of the material's energy band gap, enhancing its light absorption capabilities (Xiaochao et al., 2020). PANI can be used in different fields and is very interesting for researchers due to its high mobility of charge carriers, high conductivity, excellent stability,

high absorption co-efficiency in visible light, enhanced photocatalytic activity, biocompatibility, environmental stability and direct synthesis by chemical oxidation and electrochemical methods (Shirmardi et al., 2018). So, PANI is a good candidate to increase the photocatalytic activity of inorganic semiconductors, and also it has been successfully used to improve the performance of NiO. In our previous research, we synthesized and evaluated novel metal-decorated nanocomposites (NCs) for photocatalytic degradation of BPB and MG dye. These NCs include CdO/PANI and TiO2/PANI nanoparticles decorated with silver (Ag) and nickel (Ni) in aqueous media and wastewater effluent, respectively (Alemu et al., 2022; Alemu et al., 2023; Asefa et al., 2024). The result revealed that the maximum photocatalytic degradation efficiency was achieved at about 98% using NC systems as compared to the respective binary system showing the impact of homopolymer is paramount. The great challenge related to the use of NPs within polymer composites is the agglomeration of NPs. Such challenges would decrease their large surface area to volume ratio and decrease their effectiveness which can be solved through adopting in-situ polymerization of metal NPs in the repeating unit. It involves the simultaneous formation of metal NPs and polymer matrices within a sol-gel matrix which can be advantageous for creating NCs with unique properties through the homogeneous distribution of metal NPs within the gel matrix and the incorporation of polymer enhancing the stability of metal NPs by preventing the aggregation or precipitation during the sol-gel process (Bonomo., 2018). Moreover, the in-situ polymerization has advantages due to the simplicity, good reproducibility, and inexpensive, environmentally friendly, and easier scale-up of the process; uniformly dispersing the metal nanoparticles inside the polymer matrix (Alemu et al., 2022). Sol-gel method was preferred in this study because it is one of the simplest and cheapest techniques to prepare the metal oxides-based NPs/NCs. It could also provide a high specific surface area with uniform particle size and shape distribution in cost-effective and efficient experimental situations. However, the other techniques such as hydrothermal, solvothermal, thermal decomposition, and microwave-assisted methods require quite expensive instrumental apparatus, energy consuming/high experimental conditions, and are less efficient so that they generate unstable and large particle sizes with less crystallinity (Bonomo, 2018).

This research focused on developing nickel oxide (NiO), copper-nickel oxide (Cu-NiO), and copper-nickel oxide/polyaniline (Cu-NiO/PANI) nanomaterials using a sol-gel method. We characterized these materials using FT-IR, XRD, and UV-VIS spectroscopy. Additionally, we investigated how factors like irradiation time, pH, dye concentration, catalyst amount, and reaction temperature affect their ability to degrade a pollutant through photocatalysis of Tris(4-(Dimethylamino) Phenyl) Methylium Chloride (TDPM) dyes with its degradation mechanisms. Thus, it is expected that the current study would offer significant information about the optimum working conditions by preparing cost-effective and suitable alternatives for industrial wastewater treatment processes.

Materials and Methods

Experimental sites

The synthesis of NiO, Cu-NiO, and Cu-NiO/PANI NCs, the study of photocatalytic activity, and characterization using a UV-Vis spectrometer were done at Ambo University, College of Natural and Computational Sciences, Chemistry Research Laboratory. The synthesized NCs were further characterized using XRD and FTIR at Adama and Addis Ababa Science and Technology University, respectively.

Chemicals, Apparatus, and instruments

The chemicals used for this study were Tris(4-(Dimethylamino)Phenyl)Methylium Chloride (TDPM) dye, copper chloride (CuCl2), nickel nitrate (Ni(NO3)2).6H2O), methanol (98%, Merck), sulfuric acid (H2SO4) (98%), hydrochloric acid (HCl), ammonium persulfate (APS, (NH4)2S2O8, 98%), aniline monomer

(C3H7NO2) (98%) (All Chemical were purchased from Sigma Aldrich Chemical) and distilled water were used throughout this experiment to prepare NiO, Cu-NiO and Cu-NiO/PANI photocatalysts. All reagents and chemicals used were analytically graded and used without further purification. The band gaps of all developed NCs were determined by UV-visible spectroscopy (Dell, model, company, and country), the structures of synthesized nanomaterial were examined by the powder X-ray diffractometric techniques X-ray Diffractometer (XRD, Shimadzu XRD-7000, German), and the functional groups of developed NCs were determined by Fourier-transform infrared spectroscopy (FT-IR, Shimadzu 8400S, German) spectroscopy.

Synthesis of NiO NPs and Cu-NiO NPs

In the sol-gel process, 15 g of Ni (NO3)2.6H2O was transferred to the first beaker and dissolved in 200 mL of distilled water (DI water) at room temperature. In the second beaker, 5 g NaOH was dissolved in 100 mL of DI water and then added to the Ni (NO3)2.6H2O solution which was stirred for 20 min at room temperature till the mixture was transformed into a light green precipitate. The precipitate was filtered after 12 hrs. washed thoroughly with DI and finally taken into the oven and dried at 110 0C for 24 hrs. The precipitate was dried and formed a green color. Then, the dried green solid was calcinated at 400 0C for 1 hr. and obtained black powder (Bonomo, 2018). The product was collected in a sample holder and kept in desiccators for further use. Cu-NiO NPs were prepared through an addition of 3 g of CuCl2 to the solution of the above method.

Synthesis of Cu-NiO/PANI NCs

The NCs-based PANI was prepared by in-situ chemical oxidative polymerization of aniline monomer with Cu-NiO NPs in an aqueous solution of ammonium persulfate (APS) A 3 g of Cu-NiO NPs was added to 300 mL of 1M H2SO4, 3 mL of aniline was added dropwise to the solution and stirred for 30 min until a green light color was formed. A solution of 6 g APS oxidant in 300 mL of 1 M H2SO4 solution was added dropwise under a refrigerator and stirred for 30 min. The solution was changed into dark green colors which confirmed the formation of Cu-NiO/PANI NCs which was kept at room temperature for 24 hrs. The solution was filtered and washed with DI water until the filtrate became colorless. The precipitate material was filtered and dried in a vacuum oven at 80 ºC for 6 hrs. The product was collected in a sample holder and kept in desiccators for further use (Alemu et al., 2023; Asefa et al., 2024).

Characterization of Photocatalysts

The synthesized photocatalysts were subjected to XRD equipped with the graphite monochromatized (Ni-filtered) Cu-Kα radiation (λ = 1.5406 Å) in 2θ angle ranging from 10o to 80o with a step size of 0.05o and scanning rate of 2o per min for structural order determination have been done at Adama Science and Technology University while its functional groups were determined by FT-IR spectroscopy in the wave number range of 400-4000 cm-1 at Addis Ababa Science and Technology University.

From the XDR data, the crystalline structure has been measured Debye-Scherer's Eq. (2.1) **(**Zeid, Ibrahem, Ali, & Mohamed, 2019**):**

$$D = {}^{0.9\lambda}/_{\beta cos\theta} \quad \text{---------- (2.1)}$$

where λ -wavelength of radiation used in Cu K_{α} (0.15406 nm), β – full width at half-maximum of the peak, and θ - angle at the position of the maximum peak (in rad).

The energy band gap of as-synthesized photocatalysts was determined using Eq. (2.2). The absorbance of the photocatalyst in the solid states was measured using a plate by scanning over 200-800 nm **(**Alemu et al., 2022**).**

$$E_g = {}^{hc}/_{\lambda}\, eV \quad \text{---------- (2.2)}$$

where h - Plank's constant (6.62 x 10^{-34} J.s), C - speed of light (3.0 x 10^{8} m.s^{-1}) and λ is irradiation light wavelength in nm.

Effect of Operational Parameters on Photodegradation of TDPM dye

The effect of the initial concentration of model dye was studied by varying the concentration of TDPM from 10 ppm to 20, 30, and 40 ppm, catalysis load from 50 mg to 70, 90, 110, and 130 mg, pH from 3 to 5, 7, 9 and 11 while the irradiation time changed from 0 min (dark place) to 30, 60, 90, 120, 150 and 180 min at NiO, Cu-NiO and Cu-NiO/PANI surface. It was exposed to UV-Vis light and its effect on the rate of decolorization was studied. The effects of photocatalysts' dose were studied through changing the amount of catalysts from 50 mg to 130 mg keeping the initial concentration of model dye to 10 ppm, pH to 3, and irradiation time of 30 min. The effect of pH values (3, 5, 7, 9, and 11) was determined by keeping the optimum catalyst load of 110 mg, 10 ppm of initial concentration of dye, and 30 min irradiation time while the effect of irradiation time was studied through scanning the absorbance at 0, 30, 60, 90, 120, 150 and 180 min by taking the optimum parameters i.e., 10 ppm initial concentration of dye, 110 mg of catalyst dose and pH of 3 (Nandapure et al., 2013).

Photocatalytic Degradation of TDPM

The photocatalytic activities of photocatalysts were studied against the degradation of model dye i.e., Tris(4-(Dimethylamino)Phenyl)Methylium Chloride (TDPM). The experiments were carried out under UV-Vis light irradiation using 0.11 g of NiO, Cu-NiO, and Cu-NiO/PANI each dissolved in 10 mL of 100 ppm TDPM solution. The solution of model dye was then irradiated under UV-Vis light (λ_{max} = 560 nm wavelength, lamp15 W) following constant stirring for 30 min. The UV-Vis absorption measurements were taken and the photocatalysts were separated by centrifugation process. The suspension left after centrifugation was kept in the dark for 30 min with continuous stirring using a magnetic stirrer. Then, 10 mL of suspension was withdrawn and centrifuged for 5 min at 3000 rpm and its absorbance was measured. Decolorization was observed in terms of absorption intensity changes for model dye at maximum wavelength. The percentage of photocatalytic degradation of dye was calculated from the following equation **(**Alemu et al., 2022**).**

$$\% \, degradation = {}^{(A_o - A_t)}/_{A_o} \, x \, 100 \quad \text{------ (2.3)}$$

Where A_0 and A_t are an absorbance of dye at an initial time t_o and at time t respectively.

A Study of Degradation Kinetics

In this work, the study photodegradation kinetics of TDPM dyes is needed and vital for designing efficient, reliable, and predictable photocatalytic treatment processes for environmental remediation, particularly for the optimization of wastewater treatment **(**Sahoo, et al., 2005**).** The photodegradation kinetics of TDPM dye solutions were investigated using optimized photocatalyst load, initial concentration and pH of dye, and UV-Vis irradiation time. The photodegradation kinetics of TDPM dye by the photocatalysts under UV-Vis light can be evaluated by comparing the apparent rate constants **(**Sharma *et al., 2017***)**. The degradation kinetics is also described using pseudo-first-order (Eq. 2.4) and pseudo-second-order kinetics (Eq. 2.5) **(**Alemu et al., 2022**):**

$$\ln\left({}^{A_t}/_{A_o}\right) = K_{app1}.t \quad \text{---------- (2.4)}$$

$$^1/_{A_t} = {}^1/_{A_o} + K_{app2}.t$$ ---------- (2.5)

The thermodynamic study is used to reveal insight, optimize, and provide the mechanism of TDPM dye photo-degradation processes at Cu-NiO-based nanocatalyst surface (Cheruiyot *et al*., 2019). The effect of temperature on the rate of photodegradation reaction was determined using the temperature change of 298, 303, 308, and 313 K upon temperature increment of 10 degrees. From the Arrhenius equation, the activation energy was calculated as follows:

$$\ln k_{app} = -\frac{E_a}{RT} + lnA$$ ---------- (2.6)

Where k_{app} is an apparent rate constant, T is the temperature of the reaction, E_a is the activation energy, R is the gas constant (8.314 $Jmol^{-1}K^{-1}$) and A is the frequency constant. The thermodynamic parameters such as $\Delta S^* and\ \Delta H^*$ were calculated with the help of the Eyring-Polanyi equation **(**Konstantinou & Albanis, 2004**):**

$$ln\left(\frac{k_{app}}{T}\right) = \frac{\Delta H^*}{R}\frac{1}{T} + \ln\left(\frac{k_B}{h}\right) + \frac{\Delta S^*}{R}$$ ------ (2.7)

where T is the absolute temperature, ΔH^* is the enthalpy of activation, ΔS^* is the entropy of activation, k_B is the Boltzmann's constant and h is the planks constant.

The free energy was calculated using the following equation:

$$\Delta G^* = \Delta H^* - T\Delta S^*$$ ---------- (2.8)

Results and Discussion

Characterization of Photocatalysts

The Structural Analysis

Thermodynamic study

The characteristic peaks of XRD patterns for photocatalysts such as NiO NPs, Cu-NiO NPs, and Cu-NiO/PANI NCs were shown in Fig. 1. The result showed that the sharpness of peaks corresponds to the phase purity and crystal structure for the particular catalysts. The peaks appearing at 29.69, 31.88, 37.17, 43.22, 62.75, 75.32 and 79.22º (Firisa et al., 2022) with the respective miller indices of (110), (11−1), (111), (200), (220), (311) and (222) were corresponded to the crystal structure of pure NiO **(**Sharma et al., 2019) and well matched with the related JCPDS card number indicated by (Aliahmad *et al*., 2014) confirmed that NiO NPs was highly pure. For the Cu-NiO NPs sample, XRD spectra were observed at 29.39, 37.33, 43.16, 62.10, 75.32, and 79.39º which corresponds to the Miller indices of (110), (111), (200), (220), (311) and (222). In particular, the peak at 43.16º (200) was highly intensive signifying that the NiO NPs have successfully doped with Cu and modified without the crystalline structural distortion so that overall surface properties could be improved. After the preparation of nanocomposites (Cu-NiO/PANI), the incorporation of PANI was demonstrated with the emergence of new peaks at 20.06 and 25.05^0. The study has confirmed that as far as the catalyst surface is decorated with PANI homopolymer, it could minimize the intensity of diffraction peaks of nanocomposite compared with the pure substrate which is attributed to nanomaterials and polymer interactions so that it improves catalyst surface properties (Wang et al., 2013). The XRD patterns of Cu-NiO/PANI NCs maintain the peaks represented by the crystalline phase since the polymer undergoes interfacial interactions with Cu-NiO crystallites and the presence of Cu-NiO in PANI matrix so that it strongly affects the crystalline behavior of the formed PANI. Therefore, the NC has shown more crystalline than that of pure PANI indicating the advantage of forming advanced materials (Nandapure et al., 2013). Moreover, the average crystallite sizes (D) of as-synthesized photocatalysts were estimated in equation 2.1 and summarized in Table 1.

Table 1. Summary of average crystalline sizes of photocatalysts

Photocatalysts	2Θ/ degrees	Θ/ degrees	FWHM (β)	β (in radian)	CosΘ	Crystalline size (nm)	Average size (nm)
NiO	29.69	14.845	0.4004	0.00698	0.8538	23.2391	
	37.17	18.585	0.6805	0.01188	0.9479	12.316	15.46
	43.22	21.61	0.7885	0.01376	0.9297	10.8369	
Cu-NiO	37.33	18.665	0.5236	0.00914	0.9474	16.0148	14.22
	43.16	21.58	0.7615	0.01329	0.9299	11.2186	
	62.1	31.05	0.6012	0.01049	0.8567	15.4247	
Cu- NiO/PANI	20.06	10.03	3.9400	0.06877	0.9847	2.04762	3.50
	24.61	12.305	2.4800	0.04328	0.9770	3.27867	
	25.05	12.525	1.5800	0.02758	0.9762	5.15061	

Accordingly, the crystalline sizes (D) for NiO NPs, Cu-NiO NPs, and Cu-NiO/PANI NCs using the most intensive peaks at observed at 26.69, 37.17, and 43.22; 37.33, 43.16, and 62.10; 20.06, 24.61, and 25.05˚ were found to be 15.46, 14.22 and 3.50 nm respectively. These results are inconsistent with the prior report that investigated the degradation of BPB at CdO NP-based photocatalysts (Alemu et al., 2022).

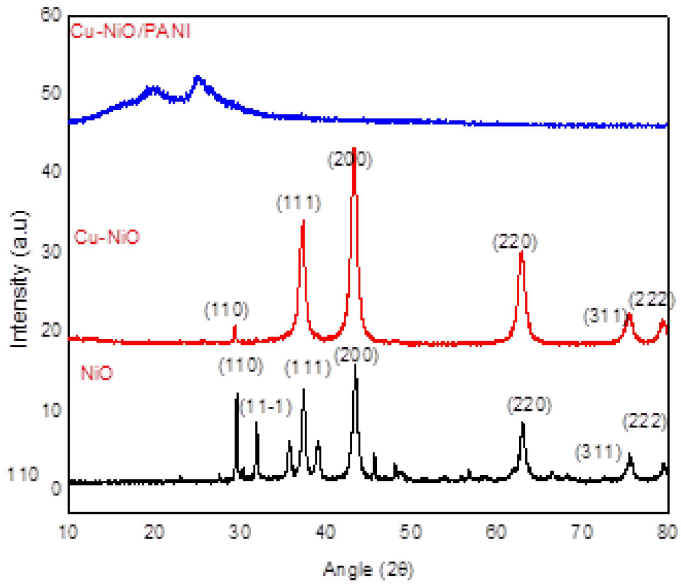

Figure 1. XRD patterns of NiO NPs, Cu-NiO NPs, and Cu-NiO/PANI NCs.

Analysis of Functional Group

Fig. 2 represents the FTIR spectrum of NiO NPs, Cu-NiO NPs, and Cu-NiO/PANI NCs. Accordingly, the absorption band displayed at 1350.49, 827.64, and 423.79 cm^{-1} represented the distinctive stretching vibrations Ni-O bond and the bending vibrations of the NiO crystal lattice structure (blue line) which agree with the spectral examined in previous studies (Nandapure et al., 2013; Nallendran et al, 2018). In the same manner, the absorption band observed around 3218.99, 1582.69, 1492.55, 1290.63, and 1089.42 cm^{-1} ascribed to the O-H stretching vibrations mode and the distinctive band for Cu-NiO NPs (Go et al., 2018). Additionally, the absorption bands demonstrated around 805.28 and 416.58 cm^{-1} correspond to the stretching vibration of Cu-O and Ni-O bonds (Kaneko et al., 2009). The FTIR spectra of Cu-NiO/PANI NCs show the main characteristic peaks at 3454, 1578, 1307, 1147, 824, 648.07, and 410.00 cm^{-1} could be attributed to N-H stretching mode (Jung et al., 2008), stretching vibrations of N=Q=N ring (Q refers to quinolinic-type rings), N-H bending modes, C-N stretching of secondary aromatic amine, the out-of-plane bending vibration of C-H on the 1,4-disubstituted aromatic rings of PANI treated NCs (Shambharkar et al., 2011) the stretching vibration of Cu-O and Ni-O, respectively (Kaneko et al., 2009) exist within the Cu doped NiO in NCs. In general, the absorption band due to stretching vibrations of quinoid rings in Cu-NiO/PANI NCs indicates the emeraldine form of oxidation state confirmed the in-situ polymerization of aniline in the presence of metal-doped semiconductor oxide. The interaction between PANI and Cu-NiO NPs has therefore been confirmed as those bands are found to be shifted in wavenumbers for Cu-NiO/PANI NCs (Nandapure et al., 2013).

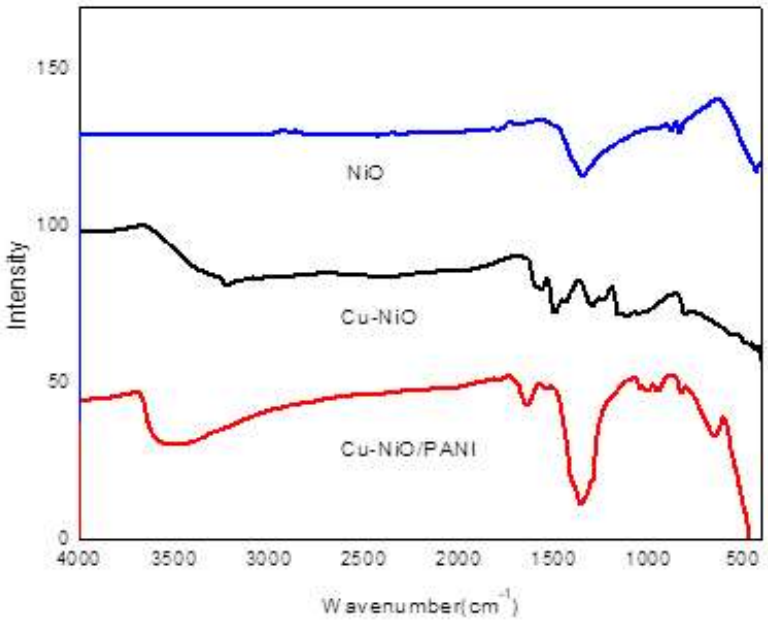

Figure 2. FT-IR spectra of NiO NPs, Cu-NiO NPs, and Cu-NiO/PANI NCs.

Determination of bandgap

In this study, the energy band gap of NiO NPs, Cu-NiO NPs, and Cu-NiO/PANI NCs was calculated from UV-Vis data using Eq. 2.2. Accordingly, the energy band gaps of NiO NPs, Cu-NiO NPs, and Cu-NiO/PANI NCs were 3.10, 1.63 and 1.60 eV respectively. The electron-hole pair generation within the catalysts is caused by the direct absorption of

photons which further causes the diffusion of the charge carriers to the surface of photocatalysts. This is probably interrelated with the lowering bandgap as a result of the formation of the dopant's energy levels below the conduction band (Gusain, Gupta, Joshi, & Khatri, 2019). The delocalized electrons of the dopant energy state account for the narrowing energy bandgap of NiO NPs from 3.60 eV to 1.63 eV upon doping with metal. Similarly, PANI promotes the shifting of wavelength to the higher value and decreases the energy band gap to 1.60 eV in Ni-CdO/PANI NCs (Figure 3). Thus, it could cause a certain fraction of holes in the VB and electrons in LUMO of PANI to be split and suppress the possibility of recombination, thus increasing the possibility of photodegradation ability as indicated in Scheme 1.

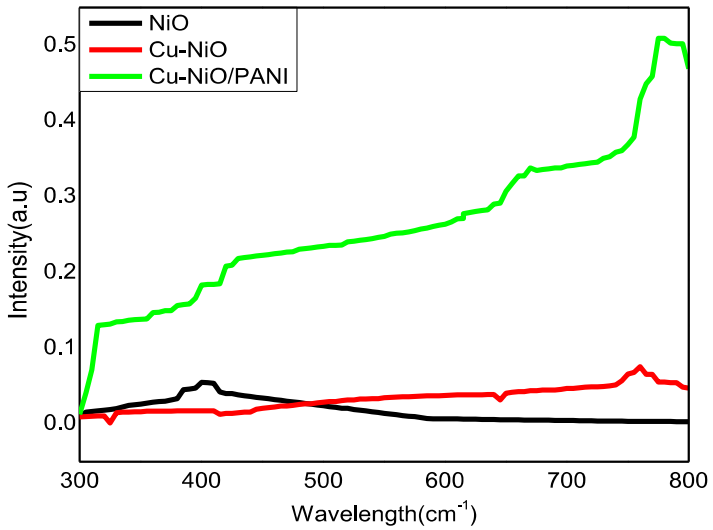

Figure 3. The UV-Vis absorption spectrum of NiO NPs, Cu-NiO NPs, and Cu-NiO/PANI NCs.

In the NCs structure, the photosensitized polymer performs the electrons-excitation from HOMO-to-LUMO which further jumped to CB of Cu-NiO NPs. An electron-accepted part would then combine with an adsorbed O_2 to form $O_2^{\cdot-}$ radicals, while $^{*}OH$ is formed due to the interaction of the holes with H_2O. The activated free radicals then effectively split the model pollutant (TDPM dye) into H_2O and CO_2 (Jana et al., 2015). Further lowering the energy bandgap of the NCs likely resulted from the synergetic effect of the addition of inorganic and organic additives that manage the crystal size and improve the nanocomposite to harvest photons (Alemu et al., 2022).

$$\text{PANI} + h\nu \longrightarrow \text{PANI}\,(e^-_{LUMO}..h^+_{HOMO})$$

$$\text{Cu-NiO/PANI} + h\nu \longrightarrow \text{Cu-NiO/PANI}\,(e^-_{LUMO}..h^+_{HOMO})$$

$$O_2 + e^- \longrightarrow O_2^{\bullet-}$$

$$O_2^{\bullet-} + 2H^+ \longrightarrow 2HO^{\bullet}$$

$$H_2O + h^+ \longrightarrow HO^{\bullet} + H^+$$

$$2HO^{\bullet} \text{ or } O_2^{\bullet-} + CV_{ads} \longrightarrow H_2O + CO_2$$

Scheme 1. The photodegradation mechanism of model dyes by Cu-NiO/PANI NCs.

Study of Photocatalytic Degradation

Fig. 4 represents the photocatalytic degradation efficiency determined by taking 10 ppm concentration of TDPM dye, 110 mg of catalysts load, pH 3, and visible light irradiation time of 210 min at room temperature, and the detailed data is shown in Table 2. Accordingly, the photocatalytic degradation efficiency of NiO NPs, Cu-NiO NPs, and Cu-NiO/PANI NCs was found to be 78.19%, 82.24%, and 96.50% respectively. The data indicated that among the three photocatalytic, Cu-NiO/PANI NCs demonstrated outstanding degradation performance at 120 min as compared to NiO and Cu-NiO NPs which ascribed to the availability of sufficient active surface area, lower energy band gap, and smaller particle sizes and thus, taken as the best photocatalyst for further optimization for degradation of TDPM dye.

Table 2. Summary of photodegradation data of photocatalysts against model dye.

Photocatalyst	**Degradation efficiency (%)**							
NiO	0 min	30 min	60 min	90 min	120 min	150 min	180 min	210
	0	51.61	70.05	70.51	72.12	77.11	78.19	78.19
Cu-NiO	0	54.51	60.10	63.61	68.05	75.60	82.24	82.24
Cu-NiO/PANI	0	63.13	67.60	94.69	96.50	95.25	95.25	95.25

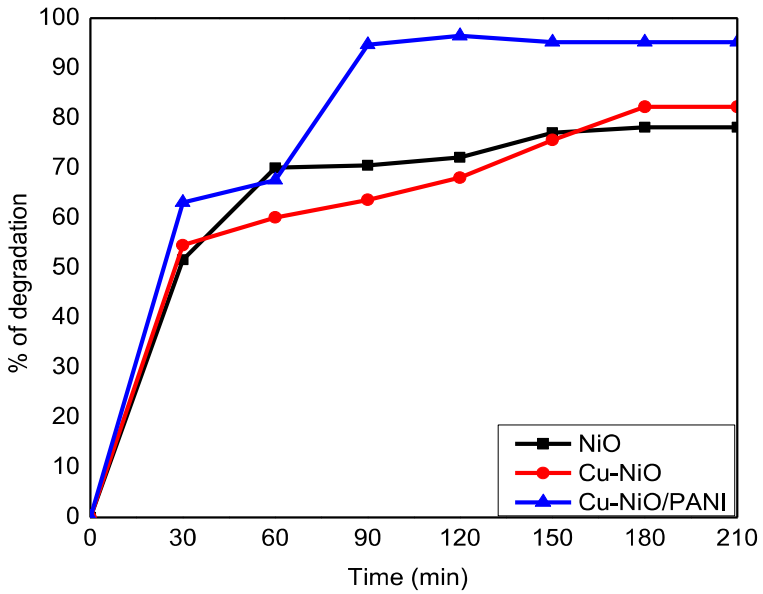

Figure 4. Comparative degradation performance of the three photocatalysts against TDPM dye.

Effect of operational parameters on photodegradation

Cu-NiO/PANI NCs Load

The effect of Cu-NiO/PANI dose has been studied by applying 50, 70, 90, 110, and 130 mg by taking 10 ppm TDPM concentration, its pH is 3, and irradiation time of 210 min at room temperature. The corresponding photodegradation efficiencies were 73.4, 87.3, 91.1, 96.5, and 96.2 respectively (Fig. 5). The photodegradation rate tended to increase with the photocatalyst dose up to 110 mg at 120 min. From the current results (Table 3), 96.50 % was the highest degradation performance recorded by Cu-NiO/PANI NCs and such immense photocatalytic efficiency was attributed to the increase in the surface active available for the degradation reaction while beyond 110 mg amount of catalyst, the number of active sites become constant which related to the decrease in light penetration as a result of shielding effect of the excessive particles and downplay surface area caused by agglomeration (Chen et al., 2010).

Table 3. Percent degradation of TDPM dye at different Cu-NiO-PANI NCs load under visible irradiation keeping pH & dye concentration at 10 ppm, 3 respectively under 25 ^{o} C.

Irradiation time/min	Cu-NiO-PANI NCs Load/mg				
	50	70	90	110	130
0	0	0	0	0	0
30	24.3	19.2	17.4	23.1	3.45
60	34.7	43.6	53.6	54.6	34
90	36.9	64.0	86.2	92.2	47.5
120	49.6	82.9	91.1	96.5	50.4
150	57.2	85.4	91.1	96.5	96.2
180	73.4	87.3	91.1	96.5	96.2
210	73.4	87.3	91.1	96.5	96.2

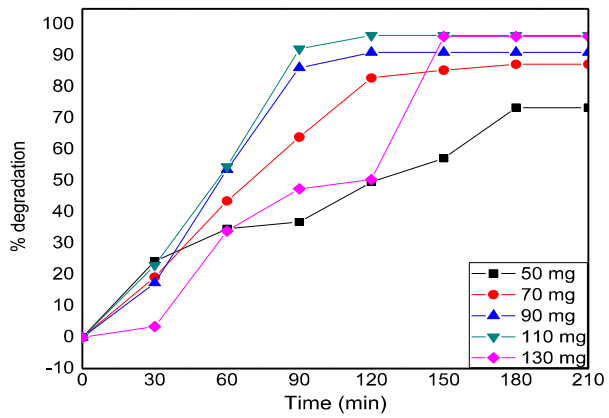

Figure 5. Photodegradation of Cu-NiO/PANI NCs against TDPM dye at different catalyst loads using irradiation light of 210 min, pH3, and dye concentration of 10 ppm at 25 °C.

Effect of pH

The effect of the solution's pH on the photodegradation of TDPM dye was determined by taking the concentration of dye, catalyst dose, and light illumination of 10 ppm, 110 mg, and 120 min respectively via taking the pH 3, 5, 7, 9 and 11 at room temperature. The observed photodegradation was found maximum in an acidic medium i.e., pH 3 provided 96.50 % photodegradation efficiency (Fig. 6). In the acidic medium, the surface catalyst becomes favorable towards the creation of free radicals as reactive intermediates so that it possibly interacts with the TDPM dye molecules and evidenced by the increased degradation reaction rate (Alemu et al., 2022). Degradation at initial pH = 1.0 was not included because, at this pH value, the dye was completely decolorized.

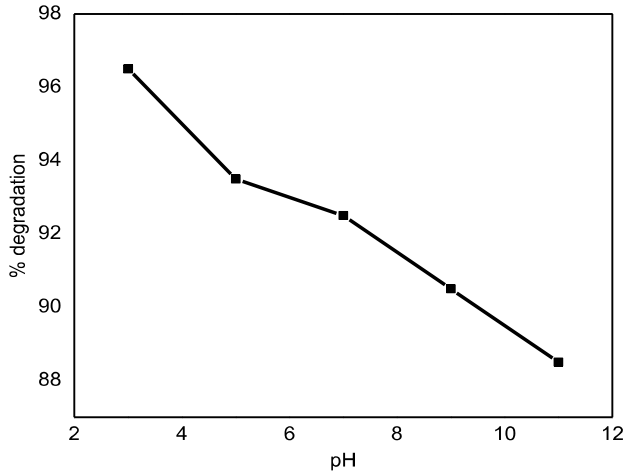

Figure 6. Degradation of TDPM dye using Cu-NiO/PANI NCs at different pH values.

The initial concentration of Dyes

Keeping all other experimental parameters constant, the concentration of dye was changed from 10 ppm to 20, 30, and 40 ppm to determine the effect of initial TDPM dye concentration on the photodegradation performance. The photodegradation of TDPM provided the maximum efficiency of 96.5% at a10-ppm concentration of dye (Fig. 7). The degradation rate tends to decrease with the gradual increases of initial concentration.. It is expected that at higher dye concentrations, the approach of the radiation photons to the catalyst surface is hindered and screened off, thereby reducing the photocatalytic activity in the system (Mehrabian, Azimirad, Mirabbaszadeh, Afarideh, & Davoudian, 2011).

Table 4: Summary of Cu-NiO/PANI NCs photodegradation performance at different initial concentrations of TDPM dye.

	Degradation			
Time/min	10 ppm	20 ppm	30 ppm	40 ppm
0	0	0	0	0
30	58.8	57.6	59.9	57.2
60	64.5	61.5	66.4	61.6
90	91.6	73.8	78.2	78.0
120	96.5	76.9	82	80.4
150	96.3	82.7	82.3	87.3
180	96.3	81.8	81.8	82.4
210	96.3	81.8	81.8	82.4

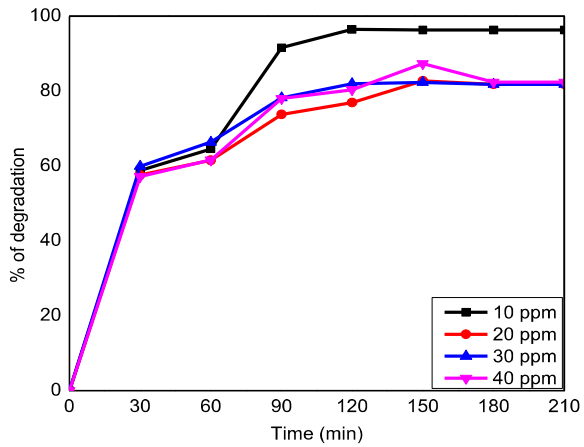

Figure 7. The degradation performance of Cu-NiO/PANI NCs at different initial dye concentrations of TDPM dye.

Study of Degradation Kinetic

Fig. 8 (a) demonstrated the pseudo-first-order reaction model for the photodegradation reaction of TDPM dye using a 10 ppm concentration of dye, pH 3, and light irradiation of 210 min. The graphical representation of $\ln(A_0/A_t)$ versus time for the pseudo-first-order rate law (Eq. 2.4) at room temperature demonstrated the apparent rate constant K_{app1} and regression coefficient (R^2) of 0.01994 min^{-1} and 0.8722 respectively. On the other hand, Fig. 7(b) displayed the plot of 1/At versus time to describe the degradation of model dye with the help of a pseudo-second-order model (Eq. 2.5) so that the apparent rate constant K_{app2} and regression coefficient (R^2) values were 0.504 $min^{-1}s^{-1}$ and 0.8751 respectively. From the two models, the degradation kinetics followed the order pseudo-second-order reaction since the correlation coefficient value has been proposed as a good criterion for selecting a kinetic model (Yu et al., 2017). These kinetic models signified the photodegradation could be increased linearly as the initial concentration of the model dye increases. Kinetically, as the TDPM dye fully adsorbed at Cu-NiO/PANI NCs surface catalyst, the degradation rate increased as well. Additionally, the advantage of PANI surface treatment has been identified

in the reduction of carrier recombination as a result of the existence of Cu NP dopant and consecutive reduction of the surface resistivity for the TDPM degradation.

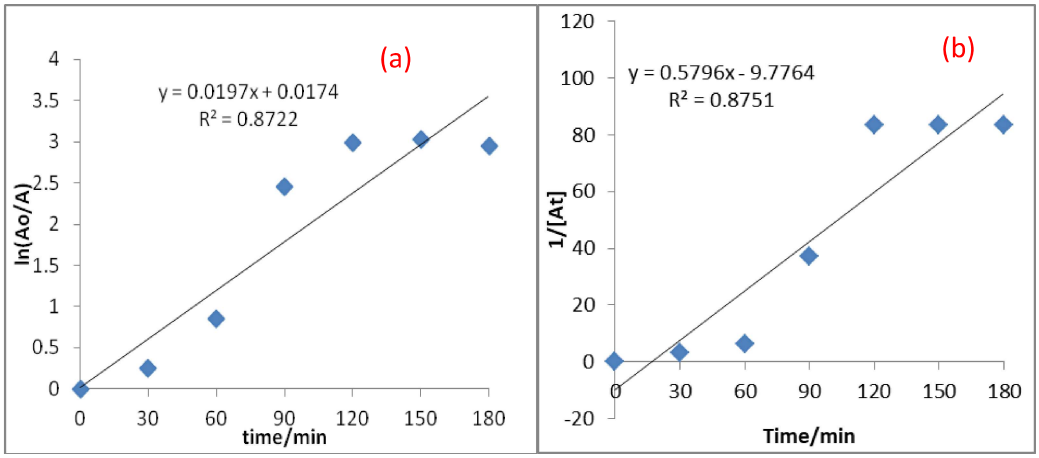

Figure 8. The graphical representation of (a) pseudo-first order reaction rate and (b) pseudo-second order reaction rate for Cu-NiO-PANI NCs.

Thermodynamic study

Fig. 9 depicts the degradation performance of Cu-NiO/PANI NCs at different temperatures. The removal efficiency of dye was decreased from 96.0 % to 26.1 % with an increase in the reaction temperature from 25 ˚C to 40 ˚C which might be owing to decreased interaction between the dye molecule and vacant active sites of Cu-NiO/PANI NCs as the temperature gets higher (Adane et al., 2015). The result indicated that the optimum temperature for degradation was 25 ºC while as the temperature is increased it leads to the inhibition of the degradation of dye due to the increased density and turbidity of the solution. Then, it would suppress the light interaction with the Cu-NiO/PANI surface and further reduce the generation of HO^* (Abbas, Hassan, & Ahmed, 2019). The thermodynamic parameters such as the activation energy (E_a), entropy of activation (ΔS^*), enthalpy of activation (ΔH^*) and free energy of activation (ΔG^*) have been calculated using Eq. (2.6-2.8) taking different temperatures values of 298, 303, 308 and 313 K. From the plot (Fig. 10) ln k versus 1/T, the straight line with slope of $-E_a/R$ was obtained.

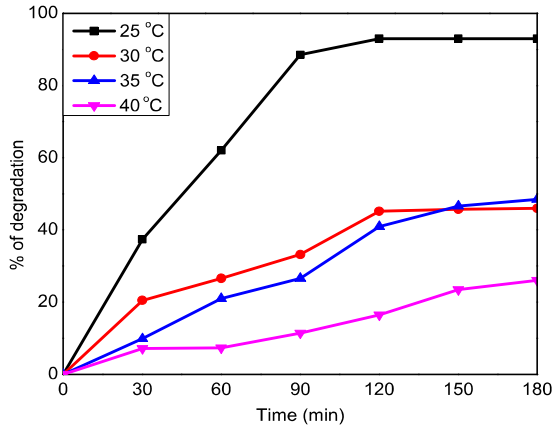

Figure 9. Degradation efficiency using different temperatures at pH 3, 10 ppm concentration of dye, and 110 mg of catalyst load.

Accordingly, E_a, ΔH^* and ΔS^* of degradation reaction are found to be 21.74, -53.7, and -0.7722 KJ/mol, respectively which implied that the transition state was highly ordered in associated with the ground state. The retention of positive numbers of the free energy of the activation implied that the reaction using the Cu-NiO/PANI catalyst for the degradation of TDPM was non-spontaneous and the extent of the non-spontaneity of the reaction increased by increasing temperature. The ΔG^* is well thought-out as a driving force of Cu-NiO/PANI surface reaction and calculated again from the value of ΔH^* and ΔS^* (Hu et al., 2010). Therefore, the ΔG^* values were positive i.e., 176.5, 180.2, 184.1, and 188.0 KJ/mol at 298, 303, 308 and 313 K, respectively. This result is in line with the proposed reaction mechanisms which was energetically unstable with a decreased reaction rate until 313 K.

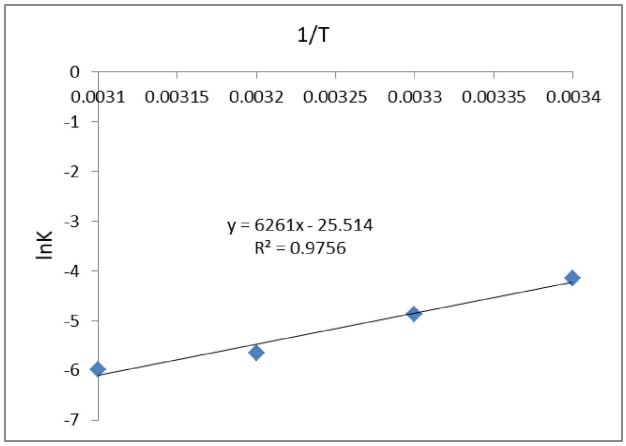

Figure 10. The curve shows the effect of temperature on the degradation of TDPM.

Conclusions

In this study, the sol-gel method was used to synthesize photocatalysts for the degradation of TDPM dye and characterized by XRD, UV-vis, and FT-IR. From UV-Vis spectroscopy, the band gap energy of NiO NPs, Cu-NiO NPs, and Cu-NiO/PANI NCs were 3.1, 1.63, and 1.60 eV respectively. The results indicate that the lowest band gap was obtained for the PANI-supported Cu-NiO NPs. Photocatalytic degradation activities suggested that Cu-NiO/PANI NCs exhibited a relatively higher efficiency on the photodegradation of TDPM dye which was about 96.5% at 10 ppm concentration of dye, pH 3, 110 mg amount of photocatalyst for 120 min light illumination whereas in case of NiO and Cu-NiO photocatalysts, only 36 % and 38 % photodegradation efficiency respectively. The photodegradation followed the pseudo-second-order kinetics with a rate constant of 0.504 $min^{-1}s^{-1}$. Thermodynamically, when the temperature was increased the dye degradation was decreased indicating that the reaction is exothermic. In general, Cu-NiO/PANI NCs demonstrated outstanding degradation capability which is a more efficient and superior photocatalyst as compared to NiO and Cu-NiO NPs and it is thus found one of the best candidates for the treatment of organic dyes.

Acknowledgments

The authors are grateful to Adama Science and Technology University, Addis Ababa Science and Technology University, and the Chemistry Department of Ambo University, Ethiopia for their support with laboratory, chemicals/reagents, and analytical instrumentals.

References

Abbas, S. K., Hassan, Z. M., & Ahmed, L. M. (2019). *Influencing the Artificial UV-A light on decolorization of Chlorazol black BH Dye via using bulk ZnO Suspensions.* Paper presented at the Journal of Physics: Conference Series.

Adane, B., Siraj, K., & Meka, N. (2015). Kinetic, equilibrium and thermodynamic study of 2-chlorophenol adsorption onto Ricinus communis pericarp activated carbon from aqueous solutions. *Green Chemistry Letters and Reviews, 8*(3-4), 1-12.

Alemu, T., Taye, G., Asefa, G., & Merga, L. B. (2022). Surface modification of Ag–CdO with polyaniline for the treatment of 3′, 3 ″, 5′, 5 ″-tetrabromophenolsulfonphthalein (BPB) under UV-visible light irradiation. *Heliyon, 8*(11), e11608.

Alemu, T., Merga, L. B., Amente, A., & Asefa, G. (2023). Treatment of wastewater dye using Ag–CdO-based nanocomposites surface modified with polyaniline. *Applied Nanoscience*, 1-13.

Aliahmad, M., Rahdar, A., & Azizi, Y. (2014). Synthesis of Cu doped NiO nanoparticles by chemical method.

Asefa, G., Negussa, D., Lemessa, G., & Alemu, T. (2024). The Study of Photocatalytic Degradation Kinetics and Mechanism of Malachite Green Dye on Ni–TiO 2 Surface Modified with Polyaniline. *Journal of Nanomaterials*, *2024*.

Bhat, S. A., Zafar, F., Mondal, A. H., Kareem, A., Mirza, A. U., Khan, S., . . . Nishat, N. (2020). Photocatalytic degradation of carcinogenic Congo red dye in aqueous solution, antioxidant activity and bactericidal effect of NiO nanoparticles. *Journal of the Iranian Chemical Society, 17*, 215-227.

Bonetto, L., Ferrarini, F., De Marco, C., Crespo, J., Guégan, R., & Giovanela, M. (2015). Removal of methyl violet 2B dye from aqueous solution using a magnetic composite as an adsorbent. *Journal of Water Process Engineering, 6*, 11-20.

Bonomo, M. (2018). Synthesis and characterization of NiO nanostructures: a review. *Journal of Nanoparticle Research*, *20*(8), 222.

Cazetta, A. L., Vargas, A. M., Nogami, E. M., Kunita, M. H., Guilherme, M. R., Martins, A. C., . . . Almeida, V. C. (2011). NaOH-activated carbon of high surface area produced from coconut shell: Kinetics and equilibrium studies from the methylene blue adsorption. *Chemical Engineering Journal, 174*(1), 117-125.

Chen, X., Shen, S., Guo, L., & Mao, S. S. (2010). Semiconductor-based photocatalytic hydrogen generation. *Chemical reviews, 110*(11), 6503-6570.

Cheruiyot, G. K., Wanyonyi, W. C., Kiplimo, J. J., & Maina, E. N. (2019). Adsorption of toxic crystal violet dye using coffee husks: Equilibrium, kinetics and thermodynamics study. *Scientific African*, *5*, e00116.

Firisa, S. G., Muleta, G. G., & Yimer, A. A. (2022). Synthesis of Nickel Oxide Nanoparticles and Copper-Doped Nickel Oxide Nanocomposites Using Phytolacca dodecandra L'Herit Leaf Extract and Evaluation of Its Antioxidant and Photocatalytic Activities. *ACS omega*, *7*(49), 44720-44732.

Go, Y., Jo, S. M., Park, S. H., Kim, H. S., You, B. S., & Kim, Y. M. (2018). Microstructure and mechanical properties of non-flammable Mg-8Al-0.3 Zn-0.1 Mn-0.3 Ca-0.2 Y alloy subjected to low-temperature, low-speed extrusion. *Journal of Alloys and Compounds, 739*, 69-76.

Gürses, A., Doğar, Ç., Yalçın, M., Açıkyıldız, M., Bayrak, R., & Karaca, S. (2006). The adsorption kinetics of the cationic dye, methylene blue, onto clay. *Journal of Hazardous Materials, 131*(1-3), 217-228.

Gusain, R., Gupta, K., Joshi, P., & Khatri, O. P. (2019). Adsorptive removal and photocatalytic degradation of organic pollutants using metal oxides and their composites: A comprehensive review. *Advances in colloid and interface science, 272*, 102009.

Hajati, S., Ghaedi, M., Mahmoudi, Z., & Sahraei, R. (2015). SnO2 nanoparticle-loaded activated carbon for simultaneous

removal of Acid Yellow 41 and Sunset Yellow; derivative spectrophotometric, artificial neural network and optimization approach. *Spectrochimica Acta Part A: Molecular and Biomolecular Spectroscopy, 150*, 1002-1012.

Hu, Q., Liu, B., Zhang, z., Song, M., & Zhao, X. (2010). Temperature effect on the photocatalytic degradation of methyl orange under UV-vis light irradiation. *Journal of Wuhan University of Technology-Mater. Sci. Ed., 25*(2), 210-213.

Imran, M., Saeed, Z., Pervaiz, M., Mehmood, K., Ejaz, R., Younas, U., ... & Hussain, S. (2021). Enhanced visible light photocatalytic activity of TiO2 co-doped with Fe, Co, and S for degradation of Cango red. *Spectrochimica Acta Part A: Molecular and Biomolecular Spectroscopy*, *255*, 119644.

Jana, B., Bhattacharyya, S., & Patra, A. (2015). Conjugated polymer P3HT–Au hybrid nanostructures for enhancing photocatalytic activity. *Physical Chemistry Chemical Physics, 17*(23), 15392-15399.

Jung, S.-H., Oh, E., Lee, K.-H., Yang, Y., Park, C. G., Park, W., & Jeong, S.-H. (2008). Sonochemical preparation of shape-selective ZnO nanostructures. *Crystal growth and design, 8*(1), 265-269.

Kaneko, F., Wada, S., Nakayama, M., Wakihara, M., Koki, J., & Kuroki, S. (2009). Capacity Fading Mechanism in All Solid-State Lithium Polymer Secondary Batteries Using PEG-Borate/Aluminate Ester as Plasticizer for Polymer Electrolytes. *Advanced Functional Materials, 19*(6), 918-925.

Katheresan, V., Kansedo, J., & Lau, S. Y. (2018). Efficiency of various recent wastewater dye removal methods: A review. *Journal of environmental chemical engineering, 6*(4), 4676-4697.

Karthik, K. V., Raghu, A. V., Reddy, K. R., Ravishankar, R., Sangeeta, M., Shetti, N. P., & Reddy, C. V. (2022). Green synthesis of Cu-doped ZnO nanoparticles and its application for the photocatalytic degradation of hazardous organic pollutants. *Chemosphere*, *287*, 132081.

Konstantinou, I. K., & Albanis, T. A. (2004). TiO2-assisted photocatalytic degradation of azo dyes in aqueous solution: kinetic and mechanistic investigations: a review. *Applied Catalysis B: Environmental, 49*(1), 1-14.

Mehrabian, M., Azimirad, R., Mirabbaszadeh, K., Afarideh, H., & Davoudian, M. (2011). UV detecting properties of hydrothermal synthesized ZnO nanorods. *Physica E: Low-dimensional Systems and Nanostructures, 43*(6), 1141-1145.

Morin, F. (1954). Electrical properties of NiO. *Physical Review, 93*(6), 1199.

Nallendran, R., Selvan, G., & Balu, A. (2018). Photoconductive and photocatalytic properties of CdO–NiO nanocomposite synthesized by a cost effective chemical method. *Journal of Materials Science: Materials in Electronics, 29*(13), 11384-11393.

Nandapure, B. I., Kondawar, S. B., Salunkhe, M. Y., & Nandapure, A. I. (2013). Magnetic and transport properties of conducting polyaniline/nickel oxide nanocomposites. *Advanced Materials Letters*, *4*(2), 134-140.

Sahoo, C., Gupta, A. K., & Pal, A. (2005). Photocatalytic degradation of Crystal Violet (CI Basic Violet 3) on silver ion doped TiO2. *Dyes and Pigments*, *66*(3), 189-196.

Saleh, R., & Djaja, N. F. (2014). Transition-metal-doped ZnO nanoparticles: synthesis, characterization and photocatalytic activity under UV light. *Spectrochimica Acta Part A: Molecular and Biomolecular Spectroscopy, 130*, 581-590.

Shah, T., Gul, T., & Saeed, K. (2019). Photodegradation of bromophenol blue in aqueous medium using graphene nanoplates-supported TiO2. *Applied Water Science, 9*(4), 1-7.

Shambharkar, B. H., & Umare, S. S. (2011). Synthesis and characterization of polyaniline/NiO nanocomposite. *Journal of Applied Polymer Science*, *122*(3), 1905-1912.

Sharma, G., ALOthman, Z. A., Kumar, A., Sharma, S., Ponnusamy, S. K., & Naushad, M. (2017). Fabrication and characterization of a nanocomposite hydrogel for combined

photocatalytic degradation of a mixture of malachite green and fast green dye. *Nanotechnology for Environmental Engineering, 2*, 1-7.

Sharma, G., Kumar, A., Sharma, S., Naushad, M., Dwivedi, R. P., ALOthman, Z. A., & Mola, G. T. (2019). Novel development of nanoparticles to bimetallic nanoparticles and their composites: A review. *Journal of King Saud University-Science, 31*(2), 257-269.

Shirmardi, A., Teridi, M. A. M., Azimi, H. R., Basirun, W. J., Jamali-Sheini, F., & Yousefi, R. (2018). Enhanced photocatalytic performance of ZnSe/PANI nanocomposites for degradation of organic and inorganic pollutants. *Applied Surface Science, 462*, 730-738.

Yu, J.-L., Zhang, S.-Q., & Hong, X. (2017). Mechanisms and origins of chemo-and regioselectivities of Ru (II)-catalyzed decarboxylative C–H alkenylation of aryl carboxylic acids with alkynes: a computational study. *Journal of the American Chemical Society, 139*(21), 7224-7243.

Yu, X., Lin, Y., Liu, H., Yang, C., Peng, Y., Du, C., . . . Zhong, Y. (2020). Photocatalytic performances of heterojunction catalysts of silver phosphate modified by PANI and Cr-doped SrTiO3 for organic pollutant removal from high salinity wastewater. *Journal of colloid and interface science, 561*, 379-395.

Zeid, E. F. A., Ibrahem, I. A., Ali, A. M., & Mohamed, W. A. A. (2019). The effect of CdO content on the crystal structure, surface morphology, optical properties and photocatalytic efficiency of p-NiO/n-CdO nanocomposite. *Results in Physics, 12*, 562-570. doi: https://doi.org/10.1016/j.rinp.2018.12.009